ISSN: 2694-1708
DOI: 10.33552/ICBC.2024.03.000552
Insights in Chemistry and Biochemistry
Iris Publishers

Research Article

Copyright © All rights are reserved by Dalila Khlaifia

Modulation of Photophysical and Structural Properties of Poly (3-Hexylthiophene) Nanowires

Dalila Khlaifia[1,2]*

[1]*Physics Department, Faculty of Arts and Sciences, Jouf University, Qurayyat 77451, Kingdom of Saudi Arabia*

[2]*Labo de Recherche 18ES19 "Synthèse Asymétrique et Ingénierie Moléculaire des Matériaux Organiques pour l'Electronique Organique" (SI2MEO), Faculty of Sciences of Monastir, University of Monastir, Tunisia*

Corresponding author: Dalila Khlaifia, Physics Department, Faculty of Arts and Sciences, Jouf University, Qurayyat 77451, Kingdom of Saudi Arabia.

Received Date: January 10, 2024

Published Date: January 24,2024

Abstract

Nanostructured conjugated polymers have been broadly exploited in organic photovoltaic devices over the past decades, as they concurrently offer the treatment advantages of polymer conductors, the photoelectric characteristics, and the nano-size effect of nanomaterials. Here, we carried out a study on the use of melt-assisted template wetting method in porous alumina membranes (AAO) to nanostructurate poly(3-hexylthiophene) (P3HT) into nanofibers. Typical sizes of these nanofibers are observed. The effects of the nanostructuration on the structural and optical properties of P3HT have been investigated by Raman spectroscopy, X-Ray Diffraction (XRD), and photoluminescence (PL). We have noticed that the nanoconfinement of P3HT into the nanopores of AAO membrane positively affects the crystallinity and the arrangement of P3HT chains.

Keywords: P3HT; Polymer; Films; Nanowires; Membrane; Properties

Introduction

Conjugated conducting polymers (CCPs) and macromolecules are a unique class of materials possessing fascinating semiconducting, chemical, mechanical, and optical properties that can be useful in a wide range of optoelectronic applications such as light-emitting diodes, photovoltaic solar cells, and lasers [1-4]. Widespread interest in nanoparticles-based on π-conjugated polymers, such as nanofiber, nanotubes, nanowires, nanorods, nanofilaments, has arisen due to their well-defined nanostructures and larger surface areas [5]. Compared to bulk CCPs, nanostructured CCPs (NCCPs) afford improved electrical conductivity, extraordinary electrochemical activity, higher carrier mobility, and enhanced optical properties [6,7]. Since structure-properties relationship is highly important for evolving the exploitation of NCCPs into high-performance devices, several fabrication strategies and techniques were developed in the last decades [8,9]. In this concept, enormous efforts have been spent on adjusting their surface, patterns, phase, and lattice fringes to encounter different requirements in various aspects. Compared to many other nanostructuring methods, template-based technique using Anodic Alumina Oxide (AAO) nanoporous membranes is a powerful method to produce highly ordered and dense networks of (1D) nanostructures with controllable morphologies such as diameter and length [10]. This strategy is widely applied in nanostructuring organic polymers and macromolecules because it enables formation of millions of nanostructures with controllable size into large-scale arrays in a cost-effective way [11,13].

The conducting polymer Poly(3-hexylthiophene) (P3HT) has been widely adopted as a polymeric hole-transporting material in organic electronic devices, due to its good crystallinity and outstanding charging carrier and hole mobility [14,15]. Owing to its excellent chemical and optoelectronic properties, the P3HT-based organic solar cells possess outstanding photovoltaic properties with high power conversion efficiencies (PCE) of 10 % [16]. As known, the performance of OSCs strongly depends on the order of the active layer [17], thus, better arrangement of CCP chains into ordered crystalline regions leads to faster charge transport and charge limited-recombination [18,19].

This work is licensed under Creative Commons Attribution 4.0 License

In this paper, we carried out a study on the use of melt-assisted template wetting method in AAO membranes to nanostructurate P3HT into nanofibers. The effects of the nanostructuration on the structural and optical properties of P3HT were discussed. We have noticed that the nanoconfinement of P3HT into the nanopores of AAO membrane positively affects the crystallinity and the arrangement of P3HT chains.

Experimental Methods and Details

In the present work, we used regioregular (rr-P3HT) purchased from Sigma Aldrich with a head-to-tail configuration (>95%) and a molecular weight in the range of 15000 and 45000 gmol-1. The P3HT solution was prepared in chloroform (CHCl3) in a concentration of 10 mg/ml. We then prepared nanofibers (NFs) from P3HT using melt assisted method in anodized oxide (AAO) membrane (Anodic 13, Whatman Mtd.,) with nominal pore of diameter of 200 nm and a membrane thickness of 60 µm. We started the experiment by drop-casting a volume of 80 µL of a 10 mg/mL solution of P3HT on glass. After drying, we obtained a spherical layer with a thickness of 4-6 µm which is separated from the glass support and deposited on the surface of the alumina membrane. The sample was placed in a vacuum chamber and heated at 250 °C for 30 minutes. Under the effects of temperature, the polymer diffuses into the pores of the alumina. Slow cooling at a rate of 2 °C/min to room temperature allows the solidification of the polymer within the pores. The last step of the "template-based fabrication" approach is the removal of the AAO membrane by immersing the sample in 25 wt% phosphoric acid (H3PO4) solution for 12 hours. Finally, the nanostructures were rinsed with deionized water several times.

Characterization

Scanning electron microscopy (SEM) observations were performed using a JOEL microscope (JSM-7600F) operating at 5 kV. The X-ray diffraction analysis was carried out using a SIEMENS D5000 diffractometer operating at a voltage of 40 kV and a current of 30 mA. The X-ray source used is the CU-Kα line with radiation of λ = 1.541 Å. The photoluminescence (PL) decays were acquired with a Hamamatsu C7700 streak camera.

Results and Discussion

(Figure 1) After removal of the AAO membrane using a solution of phosphoric acid (H3PO4), a droplet of the solution of nanofibers was deposited on a Si substrate. The examination of the cross-sectional SEM image of P3HT nanofibers (figure 1(a)) shows that the nanostructuration of P3HT by melt-assisted template yielded to fibrillar nanostructures with a diameter in the order of 200 nm and an average length of 55 µm in accordance with the morphological characteristic of the AAO membrane. As shown in figures 1(b) and 1(c), the P3HT nanofibers are relatively well ordered in aligned ropes and present a tubular structure with a wall thickness of about 40 nm. This observation was confirmed by TEM analyses. Figure S1 shows TEM images for a P3HT nanofiber with a diameter of 200 nm. Judging by the contrast of the TEM images (figure S1(b)), the nanofiber presents a tubular end. However, it is not possible to conclude that this tubular structure is maintained along the nanofibers (Figure 1 & 2).

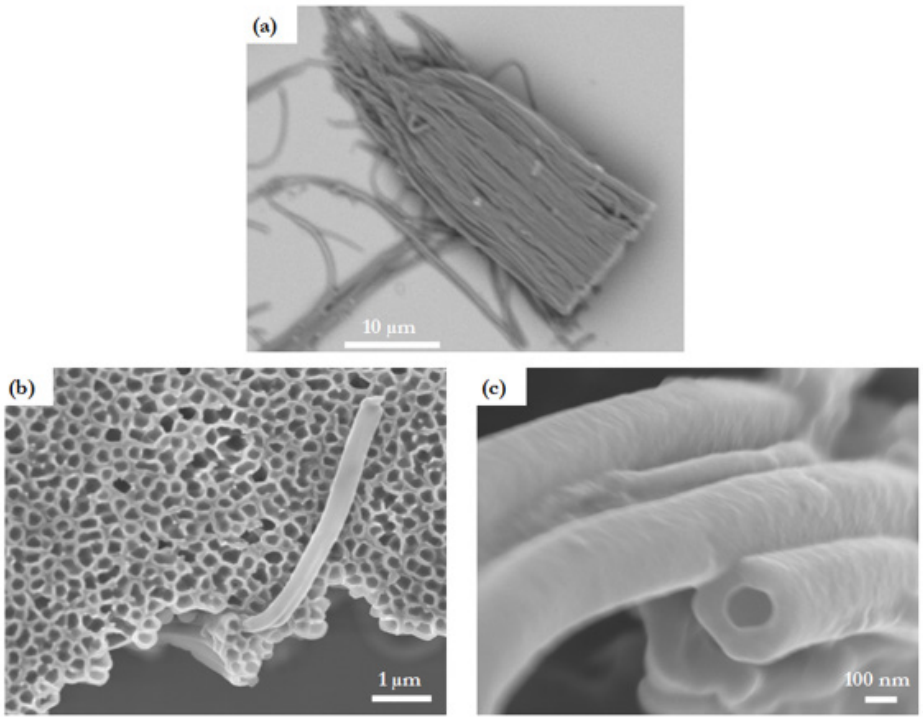

Figure 1: Scanning electron microscopy (SEM) images of nanofiber arrays of P3HT after template removal.

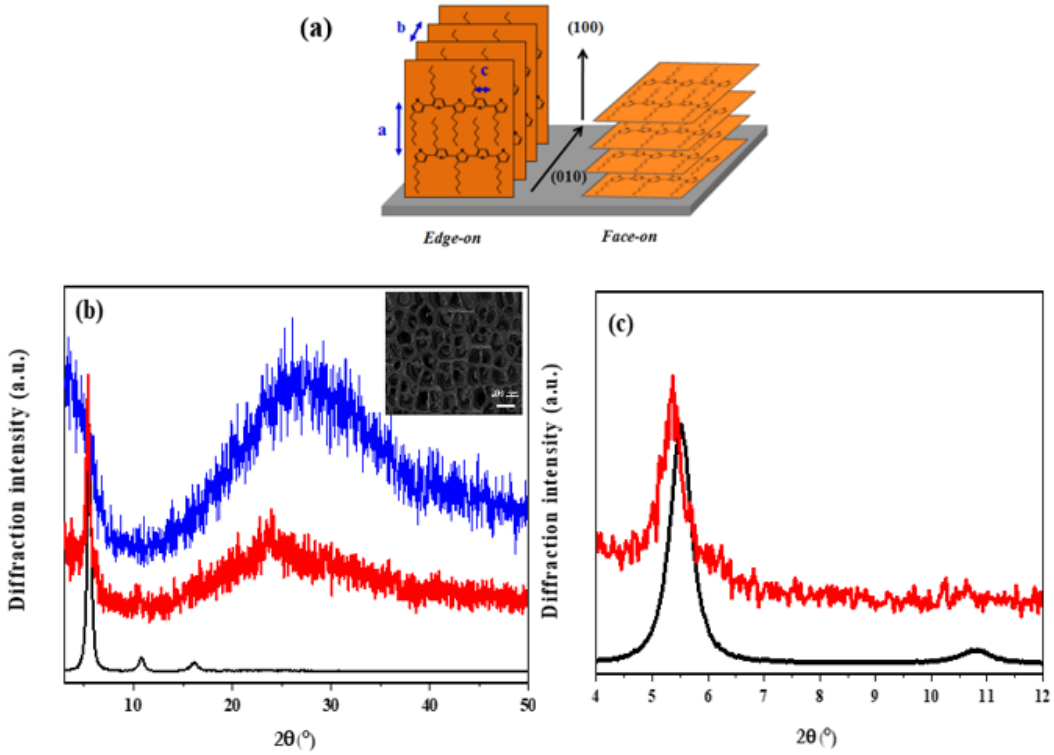

Figure 2: Schematic representation of (a) the edge-on, face-on orientations of P3HT chains (b) X-ray diffraction of a P3HT film after annealing at 250 °C for 30 minutes (black), an empty AAO membrane (blue), and a membrane impregnated with P3HT on its opposite side (Red) (the insert is the SEM image of a AAO membrane impregnated with P3HT on its impregnation side) and (c) Focus on small angles.

To further evaluate the effect of wetting template-process in the porous alumina membrane on P3HT crystallinity and chains orientation, X-ray diffraction was employed to carry out crystallinity measurements. The figure 2(b) shows the DRX diagrams, measured in Bragg-Brentano geometry, of a P3HT film deposited from a solution of 10 mg/mL heated at 250 °C for 30 minutes, an empty AAO membrane and a membrane impregnated with P3HT on its opposite side. The orientation of the membrane during the measurement was chosen to minimize the contribution of the film remaining on the surface of the membrane after impregnation (impregnation side) in the detected signal (SEM image inset figure 2(b)). As shown in figure 2(b), three main peaks around 5.52°, 10.83° and 16.14° could be resolved for the P3HT film, which are characteristics respectively to the reflection (100), (200) and (300) of P3HT [20,22]. The intensities of these peaks increased, and there 2θ values show a small shift towards lower angles in comparison to the same film before thermal treatment located at 5.67°, 10.92° and 16.41° (figure S2), which is due to the heat treatment temperature. Indeed, as previously reported in literature [23,25], the high temperature anneal improves the crystallinity within the chains networks and thereby leading to a significant increase of the crystal domains sizes.

Strong intensity of (100) peak corresponding to the lattice constant a, distance between π-conjugated backbones (Figure 2(a)), was observed suggesting the dominance of the edge-on orientation where the π-conjugated chains are parallels to the substrate while the alkyl side chains are perpendiculars to the substrate along the axis a [26]. However, we notice the absence of the peak around 23-24° assigned to the planes (010) corresponding to the lattice parameters b, indicating that the face-on configuration of P3HT is truant or negligible [26].

The XRD diagram of P3HT nanofibers in the alumina membrane shows a narrow (100) peak at 2θ = 5.37° corresponding to the edge-on chain configuration. However, comparatively to the XRD measurement on the P3HT film, the (200) and (300) peaks were not detected which could be explained by a poorer crystallinity of P3HT in the membrane. However, the (100) peak shows a shift towards the weak 2θ attributed to an increase in the lattice parameter a. In addition, the (100) width at half maximum for the P3HT nanofibers ( ) was significantly reduced compared to P3HT film ( ). Thereby using the Scherrer's relation ( ), we estimated the size of the P3HT crystallites (L) in the two cases and a value of L of about 26.51 nm was measured for the P3HT nanofibers in the membrane, compared to L=17.30 nm for the P3HT film. These results reveal an improvement in the crystallinity of P3HT after wetting in the alumina membrane. At larger 2θ, the XRD pattern of P3HT nanofibers shows a broad background originating from alumina membrane superimposed with a peak at 23.4° assigned to the planes (010), indicating face-on or vertical configuration of the P3HT chains. Consequently, this indicates that the nanoconfinement of P3HT in nanopores leads to

the appearance of a new phase oriented along the axis c in addition to the that along the axis a. Given that in our nanowires the c axis of the crystal cell (the chain orientation) points in the direction of the nanopore axis, the only orientation allowing extended-chain crystals in the pores would be the one in which the chains point in the long axis direction of the pores (Figure 3).

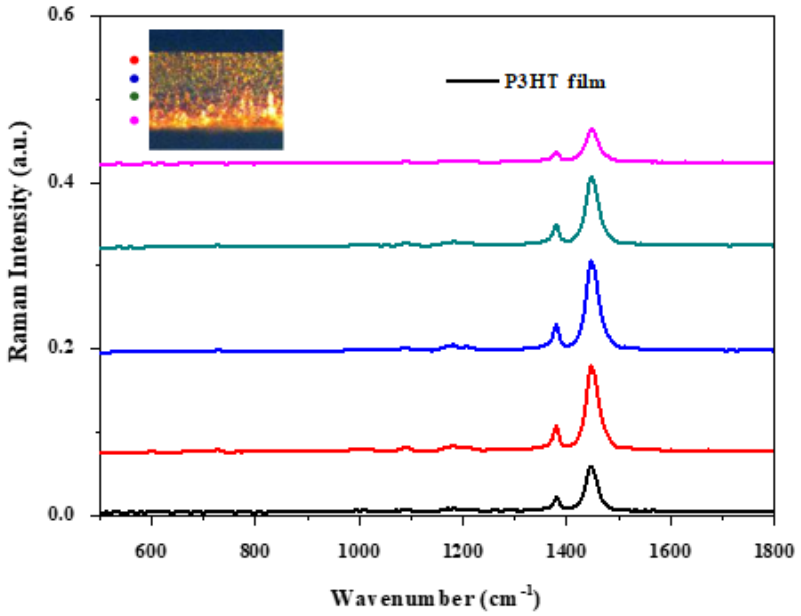

Figure 3: Raman spectra (λ exc = 1064 nm) measured on a P3HT film heated at 250°C for 30 minutes (Black) and at different positions along P3HT nanofibers embedded into the AAO membrane, as illustrated in the optical image inset. The color dots on the left side of the image show the analyzed areas from the impregnation side (red spectrum) to the opposite side of the AAO membrane, each color corresponding to a spectrum.

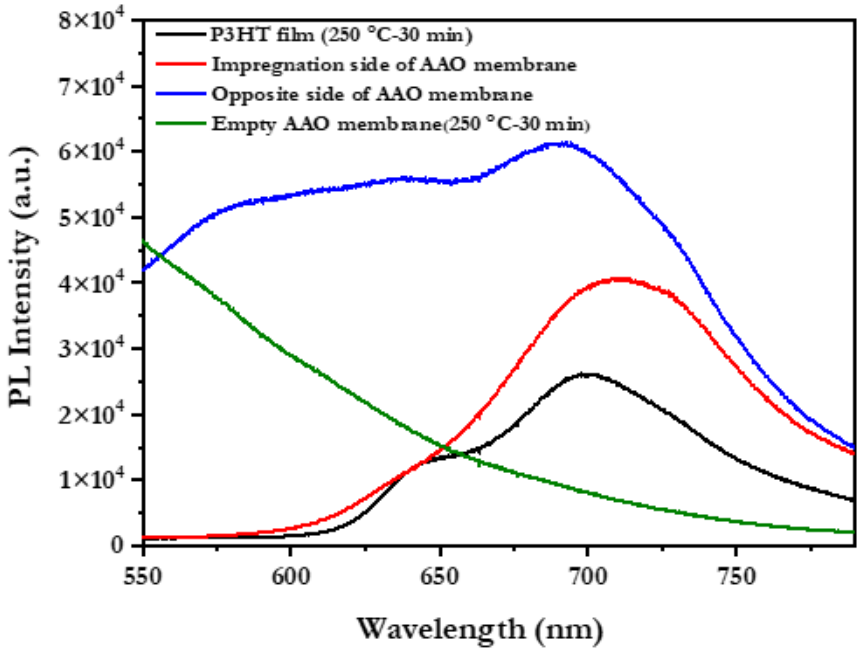

Figure 4: Photoluminescence spectra (λ excitation = 416 nm) measured on a P3HT film heated at 250°C for 30 minutes (Black), on an empty AAO membrane (green), on the impregnation side of an AAO membrane (red), and on the opposite side of the impregnation side (blue).

To elucidate the effect of the nanoconfinememt on the structural properties of P3HT, we measured the Raman spectrum of a P3HT film heated at 250°C for 30 minutes and we compared it with the Raman spectra at different positions along P3HT nanofibers embedded into the AAO membrane. The measurements were carried out using a FT-Raman (λ exc = 1064 nm) on a cross-section of an impregnated AAO membrane. As shown in figure 4, we focused on the Raman peaks at 1447 and 1380 cm-1 attributed respectively to the symmetric C=C stretching and the C-C intra-ring stretching modes characteristics of P3HT polymer [27]. As expected, the characteristics bands of P3HT show maximum intensity on the impregnation side due to the presence of the remaining P3HT film on top of the AAO membrane after the impregnation process. Then, a gradual decrease of the C=C and C-C bands was observed when going from the impregnation side to the opposite side of the AAO membrane. This decrease is mainly attributed to a progressive reduction of the amount of P3HT into the AAO nanopores, which is largely due to the presence of alumina which occupies about 40% of the volume of the AAO membrane.

Compared to the P3HT film (black spectrum), we observed an increase of intensity of C=C and C-C stretching modes peaks after impregnation of the polymer in the AAO nanopores (red spectrum). This effect can be attributed to the increase in the effective conjugation along the P3HT skeleton and then a better ordered structure of P3HT when deposited on the surface of the AAO membrane than on a glass slide (Figure 4).

Figure 4 shows the PL spectra obtained at an excitation of 416 nm of a P3HT film heated at 250°C, an empty AAO membrane, and an AAO membrane impregnated with P3HT on its face of impregnation and opposite face. For the P3HT film, the PL spectrum exhibits two main bands at 643 and 703 nm assigned, respectively, to the 0-0 and 0-1 transitions of H-aggregates in P3HT. According to the model of Spano et al. [28,29], the low 0-0 emission of P3HT is attributed to the disordered regions of the polymer which are in small portion compared to the dominant structural order [30,31].

By exciting the AAO membrane on its impregnation side and as deduced from the decomposition of the red spectrum (Figure S3), the two bands 0-0 and 0-1 bands are observed, respectively, at 660 and 708 nm. Compared to the spectrum of the P3HT film, we noticed a redshift of the luminescence as well as a decrease of the intensity of the 0-0 band. Considering that the 0-0 band at 643 nm is a signature of the disorder in the P3HT chains, the loss of its relative intensity and its shift to 660 nm can be attributed to a slightly better ordered structure of the P3HT on the remaining film on the top of the membrane after the impregnation process than that on a glass slide. As expected, for the opposite side of the AAO membrane where we excited the P3HT nanofibers and the alumina, the PL spectrum exhibited a blue shift and peak broadening indicating significant changes in 0-0 and 0-1 radiative transitions of P3HT. Indeed, the PL spectrum spreads over a wide range of wavelengths between 550 and 750 nm, which can be explained by the significant contribution of the PL of alumina which is optically very active in the range between 550 and 600 nm as shown in the blue spectrum in figure 3. Accurately, the decomposition of the blue spectrum presented in figure S3 shows two bands around 633 and 700 nm corresponding, respectively, to the 0-0 and the 0-1 transitions of P3HT. This observation validates the formation of nanofibers of P3HT in the pores of the AAO template.

Conclusion

This work aimed to study the effects of the nanoconfinement of P3HT by a template melt-assisted process. The underlying goal is the control and the ability to modulate the structural and optical properties of P3HT. The studies have focused on the effects of heat treatment at 250 °C (used during the impregnation of the nanoporous AAO membrane), as well as the effect of nanoconfinement on the organization and the optical and spectroscopic properties of P3HT. Several significant results have been achieved. We confirmed the improvement of the crystallinity of P3HT during the heat treatment at 250 °C. A morphological and spectroscopic study showed the formation of tubular type P3HT nanofibers with an average length of 55 µm and a diameter in the range 200-250 nm.

Acknowledgement

None.

Conflict of Interest

No Conflict of interest.

References

1. K N and Rout C S (2021) Conducting polymers: a comprehensive review on recent advances in synthesis, properties, and applications RSC Advances 11: 5659-97.
2. Scrosati B (1991) Conducting Polymers and Their Applications, MSF 42: 207-209.
3. Mishra A K (2018) Conducting Polymers: Concepts and Applications Journal of Atomic Molecular, Condensate and Nano Physics 5: 159–93.
4. Harun M H, Saion E, Kassim A, Yahya N, Mahmud E (2007) Conjugated Conducting Polymers: A Brief Overview.
5. Xue Y, Chen S, Yu J, Bunes B R, Xue Z, et al. (2020) Nanostructured conducting polymers and their composites: synthesis methodologies, morphologies and applications Journal of Materials Chemistry C 8: 10136–59.
6. Baig N, Kammakakam I, Falath W (2021) Nanomaterials: a review of synthesis methods, properties, recent progress, and challenges Materials Advances 2: 1821–71.
7. Abdel-Karim R, Reda Y, Abdel-Fattah A (2020) Review—Nanostructured Materials-Based Nanosensors Journal of the Electrochemical Society 167: 037554.
8. Anusiya G, Jaiganesh R (2022) A review on fabrication methods of nanofibers and a special focus on application of cellulose nanofibers Carbohydrate Polymer Technologies and Applications 4: 100262.
9. Lu Y, Shah K, Xu J (2017) Synthesis, Morphologies and Building Applications of Nanostructured Polymers Polymers 9: 506.
10. Gerrard EJP, Nurshahidah A, Derek F (2011) Progress in Nano-Engineered Anodic Aluminum Oxide Membrane Development, Materials 4: 487-526.
11. Martin C R (1994) Nanomaterials: A Membrane-Based Synthetic Approach Science 266: 1961–6.
12. Lee S B, Mitchell D T, Trofin L, Nevanen T K, Söderlund H, et al. (2002) Antibody-Based Bio-Nanotube Membranes for Enantiomeric Drug Separations Science, New Series 296: 2198-200.

13. Lee W, Park S-J (2014) Porous Anodic Aluminum Oxide: Anodization and Templated Synthesis of Functional Nanostructures Chemical Reviews 114: 7487–556.

14. Liang J, Ouyang X, Cao Y (2022) Interfacial and confined molecular-assembly of poly(3-hexylthiophene) and its application in organic electronic devices Science and Technology of Advanced Materials 23: 619–32.

15. Zhang Y, Elawad M, Yu Z, Jiang X, Lai J et al. (2016) Enhanced performance of perovskite solar cells with P3HT hole-transporting materials via molecular p-type doping RSC Advances, 6: 108888–95.

16. Chatterjee S, Jinnai S and Ie Y (2021) Nonfullerene acceptors for P3HT-based organic solar cells Journal of Materials Chemistry A 9: 18857–86.

17. Kodali HK, Ganapathysubramanian B (2012) A computational framework to investigate charge transport in heterogeneous organic photovoltaic devices. Computer Methods in Applied Mechanics and Engineering: 247–248, 113–129.

18. Zhai L, Khondaker SI, Thomas J, Shen C, McInnis M (2014) Ordered Conjugated Polymer Nano- and Microstructures: Structure Control for Improved Performance of Organic Electronics. Nano Today 9: 705–721.

19. Thompson BC, Fréchet JMJ (2008) Polymer–Fullerene Composite Solar Cells. AngewandteChemie International Edition 47: 58–77.

20. Erb T, Zhokhavets U, Gobsch G, Raleva S, Stühn B, et al. (2005) Correlation Between Structural and Optical Properties of Composite Polymer/Fullerene Films for Organic Solar Cells. Advanced Functional Materials 15(7): 1193–1196.

21. Erb T, Raleva S, Zhokhavets U, Gobsch G, Stühn B, et al. (2004) Structural and Optical Properties of Both Pure poly(3-Octylthiophene) (P3OT) and P3OT/fullerene Films. Thin Solid Films 450(1): 97–100.

22. Zen A, Saphiannikova M, Neher D, Grenzer J, Grigorian S, et al. (2006) Effect of Molecular Weight on the Structure and Crystallinity of Poly(3-Hexylthiophene). Macromolecules 39(6): 2162–2171.

23. Yang X, Loos J, Veenstra SC, Verhees WJH, Wienk MM, et al. (2005) Nanoscale Morphology of High-Performance Polymer Solar Cells. Nano Letters 5(4): 579-583.

24. Ma W, Yang C, Gong X, Lee K, Heeger AJ (2005) Thermally Stable, Efficient Polymer Solar Cells with Nanoscale Control of the Interpenetrating Network Morphology. Advanced Functional Materials 15(10): 1617-1622.

25. Li L, Lu G, Yang X (2008) Improving Performance of Polymer Photovoltaic Devices Using an Annealing-Free Approach via Construction of Ordered Aggregates in Solution. Journal of Materials Chemistry 18(17): 1984-1990.

26. Aryal M, Trivedi K, Hu W (2009) Nano-Confinement Induced Chain Alignment in Ordered P3HT Nanostructures Defined by Nanoimprint Lithography. ACS Nano 3(10): 3085–3090.

27. Tsoi WC, James DT, Kim JS, Nicholson PG, Murphy CE, et al. (2011) The Nature of In-Plane Skeleton Raman Modes of P3HT and Their Correlation to the Degree of Molecular Order in P3HT:PCBM Blend Thin Films. Journal of American Chemical Society 133: 9834-9843.

28. Martín J, Nogales A, Martín-González M (2013) The Smectic–Isotropic Transition of P3HT Determines the Formation of Nanowires or Nanotubes into Porous Templates. Macromolecule 46: 1477–1483.

29. O'Carroll D, Lieberwirth I, Redmond G (2007) Melt-Processed Polyfluorene Nanowires as Active Waveguides. Small 3: 1178–1183.

30. Sun X, Xu F, Li Z, Zhang W (2006) Photoluminescence properties of anodic alumina membranes with ordered nanopore arrays, Journal of Luminescence 121: 588–94.

31. Li G H, Zhang Y, Wu Y C, Zhang L D (2003) Wavelength dependent photoluminescence of anodic alumina membranes Journal of Physics: Condensed Matter 15: 8663-71.